

# Biogeochemical timescales of climate change onset and recovery in the North Atlantic interior under rapid atmospheric CO<sub>2</sub> forcing

Leonardo Bertini<sup>1</sup> and Jerry Fong Tjiputra<sup>2</sup>

<sup>1</sup>University of Bergen

<sup>2</sup>NORCE

November 24, 2022

## Abstract

Anthropogenic climate change footprints in the ocean go beyond the mixed layer depth, with considerable impacts throughout mesopelagic and deep-ocean ecosystems. Yet, little is known about the timing of these environmental changes, their spatial extent, and the associated timescales of recovery in the ocean interior when strong mitigation strategies are involved. Here, we simulate idealized rapid climate change and mitigation scenarios using the Norwegian Earth System Model (NorESM) to investigate timescales of climate change onset and recovery and the extent of change in the North Atlantic (NAtl) interior relative to Pre-industrial (PI) variability across a suite of environmental drivers (Temperature – T; pH; Dissolved Oxygen – DO; Apparent Oxygen Utilization - AOU; Export Production - EP; and Calcite saturation state -  $\Omega_c$ ). We show that, below the subsurface domains, responses of these drivers are asymmetric and detached from the anthropogenic forcing with large spatial variations. Vast regions of the interior NAtl experience detectable anthropogenic signal significantly earlier and over a longer period than those projected for the subsurface. In contrast to surface domains, the NAtl interior remains largely warmer relative to PI (up to +50%) following the mitigation scenario, with anomalously lower EP, pH and  $\Omega_c$  (up to -20%) south of 30°N. Oxygenation in the upper mesopelagic of up to +20% is simulated, mainly driven by a decrease in consumption during remineralization. Our study highlights the need for long-term commitment focused on pelagic and deep-water ecosystem monitoring to fully understand the impact of anthropogenic climate change on the North Atlantic biogeochemistry.

1 **Biogeochemical timescales of climate change onset and**  
2 **recovery in the North Atlantic interior under rapid**  
3 **atmospheric CO<sub>2</sub> forcing**

4  
5 Leonardo Bertini<sup>1,2</sup>, Jerry Tjiputra<sup>3</sup>

6  
7 <sup>1</sup> University of Bergen, Faculty of Mathematics and Natural Sciences, Department of Biological  
8 Sciences, Bergen, Norway

9 <sup>2</sup> Ghent University, Marine Biology Research Group, Krijgslaan 281, B-9000, Gent, Belgium

10 <sup>3</sup> NORCE Norwegian Research Centre, Bjerknes Centre for Climate Research, Bergen, Norway

11  
12 Corresponding author: Jerry Tjiputra (jetj@norceresearch.no)

13 **Key Points:**

14  
15 - Projections reveal complex and spatially heterogeneous responses of interior  
16 biogeochemical drivers to strong CO<sub>2</sub> increase and mitigation

17  
18 - In many parts of the North Atlantic interior, detectable anthropogenic change signals occur  
19 earlier than in the upper ocean

20  
21 - In regions of relatively rapid change, interior recoveries are slower than at surface domains,  
22 mediated by changes from the South Atlantic.

23  
24  
25 **Plain language summary**

26  
27 Widespread climate change and increasing CO<sub>2</sub> emissions have effects that go beyond the  
28 ocean surface, impacting ecosystems in the deep ocean. However, the timing of changes is  
29 poorly understood, let alone where particularly responsive or unresponsive areas occur  
30 following mitigation towards Pre-Industrial atmospheric CO<sub>2</sub>. We use a computer model  
31 called NorESM to simulate the planet and its major physicochemical, geological and  
32 biological processes in the atmosphere, hydrosphere and lithosphere. We forced the model  
33 with strong and steady injection followed by strong removal of atmospheric CO<sub>2</sub> back to Pre-  
34 Industrial levels to understand the responses of seawater properties in the North Atlantic  
35 interior (Temperature, pH and Dissolved Oxygen). We find that southern portions of the  
36 North Atlantic interior remained up to 50% warmer and inhospitable to calcifying organisms  
37 even after returning the atmosphere to the Pre-Industrial state and allowing time for the  
38 oceans to readjust. A counterintuitive accumulation of oxygen in the ocean interior is also  
39 observed, despite reduced solubility in warmer seawater temperatures, mainly driven by  
40 reduced export and consumption of organic matter at depth. Further studies are needed to  
41 better understand the impact of anthropogenic climate change mitigation strength to  
42 safeguard the ecosystems of the deeper parts of our oceans.

43 **Abstract**

44

45 Anthropogenic climate change footprints in the ocean go beyond the mixed layer depth, with  
46 considerable impacts throughout mesopelagic and deep-ocean ecosystems. Yet, little is  
47 known about the timing of these environmental changes, their spatial extent, and the  
48 associated timescales of recovery in the ocean interior when strong mitigation strategies are  
49 involved. Here, we simulate idealized rapid climate change and mitigation scenarios using  
50 the Norwegian Earth System Model (NorESM) to investigate timescales of climate change  
51 onset and recovery and the extent of change in the North Atlantic (NAtl) interior relative to  
52 Pre-industrial (PI) variability across a suite of environmental drivers (Temperature – T; pH;  
53 Dissolved Oxygen – DO; Apparent Oxygen Utilization - AOU; Export Production - EP; and  
54 Calcite saturation state -  $\Omega_c$ ). We show that, below the subsurface domains, responses of  
55 these drivers are asymmetric and detached from the anthropogenic forcing with large spatial  
56 variations. Vast regions of the interior NAtl experience detectable anthropogenic signal  
57 significantly earlier and over a longer period than those projected for the subsurface. In  
58 contrast to surface domains, the NAtl interior remains largely warmer relative to PI (up to  
59 +50%) following the mitigation scenario, with anomalously lower EP, pH and  $\Omega_c$  (up to -20%)  
60 south of 30°N. Oxygenation in the upper mesopelagic of up to +20% is simulated, mainly  
61 driven by a decrease in consumption during remineralization. Our study highlights the need  
62 for long-term commitment focused on pelagic and deep-water ecosystem monitoring to fully  
63 understand the impact of anthropogenic climate change on the North Atlantic  
64 biogeochemistry.

65

66 **Keywords:** ESM, oxygenation, Biogeochemistry, climate change, mesopelagic North

67 Atlantic, time of emergence, recovery timescales, marine ecosystem

68

69 **1. Introduction**

70

71 Ocean biogeochemistry is expected to change because of future climate change, with  
72 apparent consequences for marine ecosystem services that are essential for human  
73 well-being [IPCC, 2019]. These changes are a result of direct and indirect impacts on the  
74 climate system and involve not only warming due increasing greenhouse gases but also  
75 subsequent changes in the large-scale circulation of the global ocean. Many studies  
76 investigating future climate change projections have highlighted that it is not just the  
77 surface and subsurface layers of the oceans which are subject to significant change  
78 because of anthropogenic forcing. The ocean interior is also affected by either direct or  
79 indirect effects of global warming as the oceans become more stratified and the main  
80 gateways for deep ocean ventilation and rates of heat and carbon sinks are  
81 compromised [Caesar *et al.*, 2020; Gehlen *et al.*, 2014; Sarmiento and Le Quere, 1996].

82

83 The North Atlantic (NAtl) is one of the regions of great interest to study the long-term  
84 effects of climate change given its close coupling with the atmosphere. Responses of  
85 ocean biogeochemistry to climate change are expected to be particularly stronger in  
86 zones of deep convection of the NAtl with cascading effects throughout the ocean  
87 interior via changes in the Atlantic Meridional Overturning Circulation (AMOC). The  
88 thermohaline circulation in the NAtl is largely responsible for triggering the global  
89 overturning circulation and the deep ventilation via the formation of North Atlantic Deep  
90 Water (NADW), constituting the major gateway through which anthropogenic CO<sub>2</sub>  
91 penetrates the interior and deep ocean on a global scale [Tjiputra *et al.*, 2010b; Völker *et al.*,  
92 2002]. This close coupling with the atmosphere is not only strongly linked to  
93 interannual to multi-decadal climate variability [Chen and Tung, 2018] but also very  
94 sensitive to long-term climate change [Goris *et al.*, 2015; Zickfeld *et al.*, 2008].

95

96 Observational research suggests that the strength of the AMOC has decreased at an  
97 annual rate of 7% between 2004 and 2012 [Smeed *et al.*, 2014]. This is mainly attributed

98 to the melting of ice caps which leads to the freshening of seawater in subduction zones.  
99 The loss of sea-ice reduces albedo, further contributing to the increase in sea surface  
100 temperature (SST), forming a positive feedback mechanism [Box *et al.*, 2012]. As a  
101 result, water column stability increases in high latitudes, which translates not only into  
102 the weakening of the AMOC but also in changes in biogeochemical properties as  
103 stratification hinders nutrient supply and affects the turnover of organic matter throughout  
104 the water column. These changes in thermohaline circulation and ocean  
105 biogeochemistry lead to decreases in ocean productivity and can ultimately disrupt  
106 marine ecosystem services that are critical to human livelihood, with impacts already  
107 evident at higher latitudes [Wassmann *et al.*, 2011]. The long-term consequences of  
108 these shifts for the global ocean carbon cycle and, in particular, the biological pump are  
109 still largely unknown, let alone the possible effects on the restructuring of biological  
110 communities in the ocean interior which depend largely on the export of particulate  
111 organic carbon (Export Production, EP) that is produced within the mixed layer [Jones *et al.*, 2014; Ramirez-Llodra *et al.*, 2011].

113  
114 Habitats of the NATl interior (i.e. the mesopelagic and deep ocean) are amongst the ones  
115 which will face the greatest challenges [Levin and Le Bris, 2015]. Not only do these  
116 regions depend largely on the organic matter sinking from well-lit layers, all benthic and  
117 demersal life forms in these environments have evolved in relatively stable conditions  
118 and withstand only small fluctuations in physical and biogeochemical properties, such as  
119 Temperature (T), Dissolved Oxygen (DO), Export Production (EP), and Calcite  
120 Saturation State ( $\Omega_c$ ). For instance, the mesopelagic NATl is home to vast communities of  
121 cold water corals (CWC), some of which are thousands of years old and stretch out for  
122 more than 30 kilometres [Buhl-Mortensen *et al.*, 2015; Costello *et al.*, 2005]. These reefs  
123 support a diverse community of commercially important fish and associated detritivores  
124 [Baillon *et al.*, 2012; Henry *et al.*, 2013]. Furthermore, the mesopelagic ocean is also  
125 home to the largest fish communities on Earth. Irigoien *et al.* [2014] suggest that the

126 biomass of mesopelagic fish could be 100 times greater than the global marine fisheries  
127 (~100 million tons - [FAO, 2018]).

128

129 Previous studies have focused on understanding how biogeochemical properties in the  
130 surface ocean are changing in the face of global warming and ocean acidification  
131 [Courtney *et al.*, 2017; Kwiatkowski *et al.*, 2020; Meyer and Riebesell, 2015; Riebesell *et*  
132 *al.*, 2018; Webster *et al.*, 2016] presumably because the epipelagic is the domain closest  
133 to human interactions and deep ocean species are less likely to be the first affected by  
134 changes in SST [Coll *et al.*, 2020]. However, given the importance of NATl interior in  
135 regulating climate change and supporting life, an assessment of climate change impacts  
136 on this domain is of great relevance [Hidalgo and Browman, 2019]. Presently, only few  
137 studies have addressed the possible effects of climate change on the biogeochemistry  
138 and biology of the mesopelagic regions of the world's ocean [Guinotte *et al.*, 2006;  
139 Hebbeln *et al.*, 2019; Hennige *et al.*, 2015; Puerta *et al.*, 2020] and little is known about  
140 the implications of climate change recovery following the implementation of strong  
141 mitigation strategies. The timescales of climate change emergence and recovery under  
142 such scenarios are poorly understood and so are the mechanisms constraining the  
143 associated spatial variations in the interior NATl [Boucher *et al.*, 2012].

144

145 It is important to consider that measures limiting future anthropogenic warming between  
146 1.5 and 2°C above preindustrial levels are unlikely to be realized considering current  
147 carbon emissions and the short time span for adjustment with respect to carbon-free  
148 societal and economical transformations [Friedlingstein *et al.*, 2014; Hofmann *et al.*,  
149 2019; Smith *et al.*, 2016; Steffen *et al.*, 2018]. Under this perspective, addressing  
150 ecosystem recovery using mitigation scenario in Earth System Models is necessary  
151 since the most representative scenarios towards achieving the current Paris Agreement  
152 target would involve negative emissions [Gasser *et al.*, 2015; Tokarska and Zickfeld,  
153 2015]. Therefore, assessing the extent with which the biogeochemistry of the NATl

154 interior will shift and whether mesopelagic ecosystems would be able to recover under  
155 such mitigation is fundamental if we are to aim for a manageable future in the framework  
156 of a Blue Economy. This will allow us to better understand the extent of interior ocean  
157 change and the subsequent effects of such a transition on marine ecosystem drivers.

158

159 Here, we analyse the biogeochemical responses from an idealized climate change  
160 scenario of rapid warming followed by rapid cooling in the NATl interior simulated by an  
161 IPCC-class Earth System Model. Our main objective is to evaluate the spatio-temporal  
162 evolution of key ecosystem drivers of temperature, ocean acidity, dissolved oxygen,  
163 particulate organic carbon export, and calcite saturation state (T, pH, DO, EP and  $\Omega_c$   
164 respectively) throughout the different phases of the simulation and the reversibility of  
165 these drivers following a strong mitigation scenario and allowing for the system to  
166 readjust after returning atmospheric CO<sub>2</sub> (CO<sub>2atm</sub>) back to preindustrial levels. More  
167 specifically, we determine: 1) the timescales associated with the onset of anthropogenic  
168 signal, 2) the extent of change throughout the different simulation phases and 3) the  
169 persistence as well as the reversibility of the anthropogenic signal after applying  
170 mitigation, focusing on the dynamics of the North Atlantic Meridional Overturning  
171 Circulation and large-scale biogeochemical feedbacks.

172

173

174

175

176 **2. Material and Methods**

177

178 **2.1 Model system: a short overview**

179

180 We employ the Norwegian Earth System Model (NorESM1-ME; *Tjiputra et al.* [2013]),

181 which consists of atmospheric, ocean, sea-ice and land modules. The horizontal

182 resolution of atmospheric and continental domains is  $\sim 2^\circ$  whilst that of oceanic and sea

183 ice is  $\sim 1^\circ$ . The atmospheric component is derived from the Oslo version of the NCAR

184 Community Atmosphere Model (CAM4-Oslo; [*Kirkevåg et al.*, 2012]). The physical

185 oceanic component is a modified version of the Miami Isopycnic Coordinate Ocean

186 Model (MICOM; *Bentsen et al.* [2013]). The biogeochemical ocean module is originated

187 from the Hamburg Oceanic Carbon Cycle model (HAMOCC; [*Maier-Reimer*, 1993]), and

188 adapted to an isopycnic framework [*Assmann et al.*, 2010; *Tjiputra et al.*, 2010a; *Tjiputra*

189 *et al.*, 2013]. A full description and evaluation of the NorESM1-ME are available in

190 *Bentsen et al.* [2013] and *Tjiputra et al.* [2013] respectively. A brief description of relevant

191 representations of biogeochemical process in the model are provided in the **Supporting**

192 **Information**.

193

194 **2.2 Experiment design**

195

196 Prior to any external forcing, NorESM1-ME was spun up under a preindustrial (PI)

197 condition (constant 284.7 ppm CO<sub>2</sub>atm) for 900 years, allowing for a quasi-equilibrium

198 state with a weak climate drift. Initial conditions for oxygen and nutrient fields were

199 derived from the World Ocean Atlas (WOA; [*Garcia et al.*, 2010a; *Garcia et al.*, 2010b]),

200 whereas dissolved inorganic carbon and total alkalinity values were obtained from the

201 Global Data Analysis Project (GLODAP) data set [*Key et al.*, 2004]. The remaining

202 biogeochemical variables in the water column are either set to zero or small but non-zero

203 values. Further information on the spin-up phase of NorESM can be found in [*Tjiputra et*

204 *al.*, 2013]. After the spin-up phase, two simulations were performed: (i) a PI control

205 (CTRL) and (ii) an anthropogenic climate change simulation.

206

207 The CTRL simulation encompasses 250 model years at a PI state. The anthropogenic  
208 simulation consists of three subsequent transient phases: Ramp-up, Ramp-down and  
209 Extension. During the Ramp-up, CO<sub>2</sub>atm is increased at a rate of 1% yr<sup>-1</sup> from the PI  
210 CO<sub>2</sub>atm level for 140 years, reaching approximately four times the PI mean value. The  
211 Ramp-down illustrates an idealized scenario of rapid negative emissions where CO<sub>2</sub>atm  
212 is reduced at a mirroring rate of -1% yr<sup>-1</sup> for another 140 years, returning to the PI  
213 baseline. This annual rate of decrease follows the standard protocol of the Carbon  
214 Dioxide Removal Model Intercomparison Project (CDRMIP [D P Keller et al., 2018]). The  
215 Extension phase involves extending the anthropogenic simulation for 200 years from the  
216 end of Ramp-down (Fig. 1a), where CO<sub>2</sub>atm is kept at the PI value to determine the  
217 long-term responses.

218

219 Although these changes in CO<sub>2</sub>atm may seem very rapid and unrealistic when compared  
220 to the observed rate [Keeling et al., 2005], they are employed to induce strong  
221 anthropogenic forcing so that anthropogenic climate change signals, both in terms of  
222 departures and recoveries, can manifest as early as possible (e.g., Schwinger and  
223 Tjiputra [2018]). Therefore, the results from this idealized scenario constitute an  
224 important tool for assessing not only the upper limits of climate change onset and climate  
225 change recovery but also the inertial responses involved in the biogeochemistry of the  
226 interior ocean over different phases of transitional forcing.

227

### 228 **2.3 Post-processing**

229

230 Here, we interpolate the NorESM1-ME outputs from its native isopycnal vertical  
231 coordinate to regular vertical level fields (see supplementary material for more  
232 information on the interpolation and **Table S1** for a list of output variables used in the  
233 study). Since the objective of this study is to understand the onset timescales and the  
234 extent of recovery in response to anthropogenic forcing, the monthly-to-seasonal

235 variability is not of interest. We have therefore converted all monthly biogeochemical  
236 fields into annual fields.

237 Apparent Oxygen Utilization (AOU) was determined by subtracting dissolved oxygen  
238 (DO) outputs from the estimated saturation concentration ( $O_{2sat}$ ), determined using T and  
239 S fields and a MATLAB 2018b routine based on functions from the Gibbs SeaWater  
240 (GSW) Oceanographic Toolbox [McDougall and Barker, 2011].

241

## 242 **2.4 Timescale analyses**

243

244 Prior to conducting any timescale analyses, timeseries for all variables were corrected  
245 for model drift by subtracting the trends in the CTRL run from the anthropogenic runs.  
246 The time-related variables presented in this study were estimated for each grid box in the  
247 model. For each grid box, a range of natural variability in time was defined as two times  
248 the standard deviation of the last 30-yr period of the CTRL run ( $2*Plsd30$ ). This envelope  
249 ( $\pm 2*Plsd30$ ) represents the natural variability range of the respective variables (T, S, DO,  
250 etc.), meaning that any sustained deviation outside this envelope during the climate  
251 change simulation originates from external anthropogenic forcing.

252

253 Our predefined natural envelope had at its centre the mean from the last 5 years of the  
254 Pre-industrial field in question ( $Plmean5$ ) and its upper and lower limits are given by  
255  $Plmean5 \pm 2*Plsd30$ . All time-scale variables were calculated using MATLAB 2018b  
256 routines (see Supporting Information).

257

258 To test how sensitive the timescales were to the adopted envelope, we have also  
259 computed timescales based on different envelope widths, i.e.,  $Plmean5 \pm 1*Plsd30$  and  
260  $Plmean5 \pm 3*Plsd30$ . The envelope based on a fluctuation of  $\pm 1*Plsd30$  represents a  
261 more restricted condition, where departures occur earlier and recoveries later.  
262 Oppositely, the envelope based on a fluctuation of  $\pm 3*Plsd30$  represents a more tolerant  
263 condition, where departures occur later and recoveries earlier (see examples in Fig. S1).

264  
265  
266  
267

#### 2.4.1 Time of Departure (ToD)

268  
269  
270  
271  
272  
273  
274

ToD is a concept similar to ToE (Time of Emergence, [Henson *et al.*, 2017; Keller *et al.*, 2014; Tjiputra *et al.*, 2018]). We used the terminology 'Time of Departure' because our analyses are based on a perspective where transient variability leaves predefined envelopes of natural variability. ToD is defined in our study as the point in time when there are at least 10 consecutive and non-returning model years outside the predefined envelope. ToD indicates the onset of the detectable anthropogenic signal when a particular grid point is exposed to conditions outside its PI natural variability.

275  
276  
277  
278

#### 2.4.2 $t_{max}$ and $Tracer_{t_{max}}$

279  
280  
281  
282  
283  
284  
285  
286

The point in time when the series reaches its minimum or maximum change after the start of the Mitigation phase (i.e., Ramp-down) is given by  $t_{max}$ . This can be understood as the turnaround point marking the onset of the mitigation phase (i.e., from model year 140, which is when the  $CO_{2atm}$  begins to decline). In the case of pH and DO, it is expected that  $t_{max}$  represent the time of the global minima, since these variables are expected to decrease with climate change and increasing  $CO_{2atm}$ , whereas for T,  $t_{max}$  represents the time of maximum warming. The values associated with  $t_{max}$  are given by  $Tracer_{t_{max}}$ , which is the maximum or minimum value experienced at a grid point over the entire simulation period.

287  
288

#### 2.4.3 Trec

289  
290  
291  
292  
293  
294

When the time-series re-enters the natural variability envelope within the duration of the experiment, Trec is defined as the first point in time when the series returns to the envelope and remains in it for at least 10 consecutive years. If the series does not show a sustained return of at least 10 years, a linear regression is calculated using the last 100 years of the Extension phase to estimate Trec (see examples in Fig. S2).

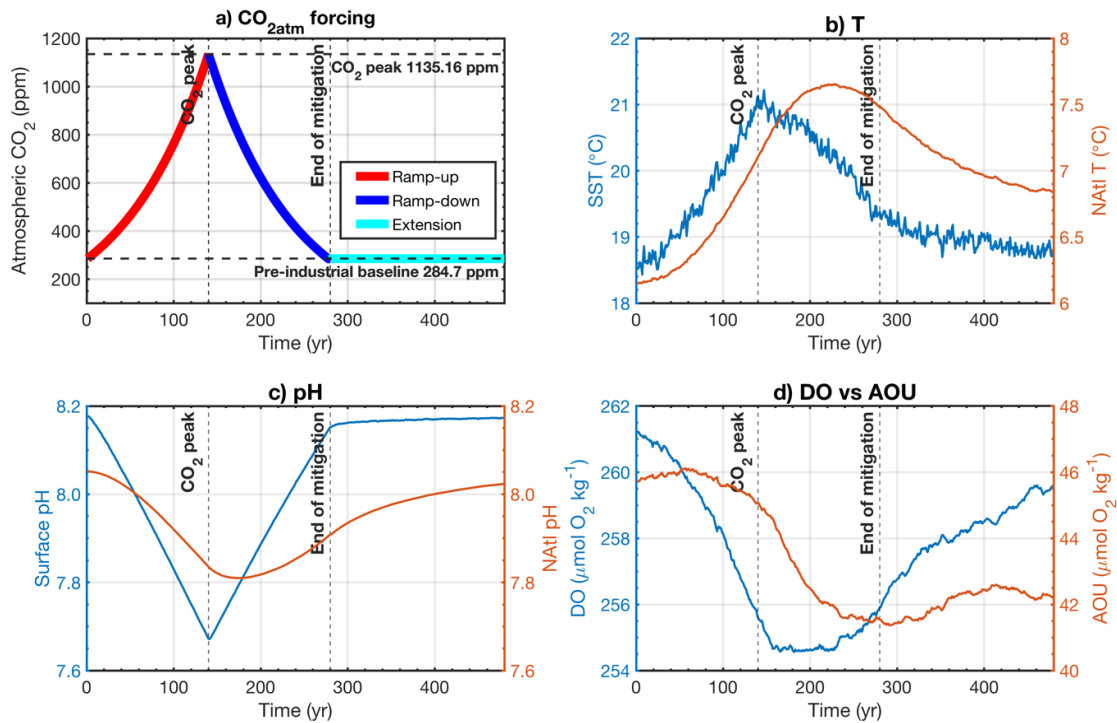
#### 2.4.4 Time-slices percentage change

To identify which regions have significantly changed over the course of the anthropogenic simulation compared to the PI, statistical analyses of percentage change of both physical and biogeochemical fields were carried out using 30-year windows (paired t-tests at a significance level  $\alpha=0.05$ ). The periods compared against the last 30 years of the PI were: a) the last 30 years of the Mitigation phase (model years 250-280), b) the middle of the Extension phase (model years 350-380) and c) the last 30 years of the Extension phase (model years 450-480). Data flagging was conducted to mark where significant changes were observed with respect to the PI. More information on the test performed and the code used are available in the [Supporting information](#).

### 3. Results

#### 3.1 Basin-scale evolution

Area-weighted and volume-weighted results for the NATl (Equator-65°N) reveal that the mean SST and the water column temperature increased by 0.13°C and 0.70°C by the end of the climate change simulation, respectively (Fig. 1b). The mean surface pH returns to the PI value while water column pH decreases by 0.025 units (Fig. 1c). The mean water column DO and AOU decrease by 1.47  $\mu\text{mol kg}^{-1}$  and 3.60  $\mu\text{mol kg}^{-1}$ , respectively (Fig. 1d). This suggests that warming and deoxygenation in the NATl relative to the PI persist, even after the Extension phase.



318

319 Figure 1 – Transient evolution of **a)** prescribed atmospheric CO<sub>2</sub> forcing; North Atlantic **b)** area-  
 320 weighted mean sea surface temperature (SST) in blue and volume-weighted mean water column  
 321 temperature (NATl T) in orange; **c)** area-weighted mean seawater surface pH in blue and volume-  
 322 weighted mean water column pH in orange and **d)** volume-weighted water column mean Dissolved  
 323 Oxygen (DO) in blue and Apparent Oxygen Utilization (AOU) in orange.

324 The evolution of the mean T vertical profile shows that thermal stratification in the  
 325 mesopelagic NATl is more pronounced 100 years after the peak of CO<sub>2atm</sub> (Fig. 2a). Our  
 326 results suggest an increase in T by as much as +3°C between 500 m and 2000 m depths. At  
 327 the end of the simulation, isotherms in the deep mesopelagic NATl are still shifted deeper by  
 328 more than 500 m from their PI position and by more than 1000 m in the deep NATl. The  
 329 evolution of the mean pH vertical profile shows that the upper mesopelagic NATl would  
 330 experience pH values as low as 7.6 for a sustained period of more than 100 years (between  
 331 model years 120 and 240), a ΔpH of -0.4 relative to PI levels. Changes in the interior NATl  
 332 down to 2000 m for the same period are also pronounced, with pH values as low as 7.7,  
 333 which also corresponds to a ΔpH of -0.4 (Fig. 2b).

334

335 Regarding the evolution of the mean DO vertical profile, the expansion of the oxygen  
 336 minimum zone is evident in the upper mesopelagic NATl up to model year 300, where levels

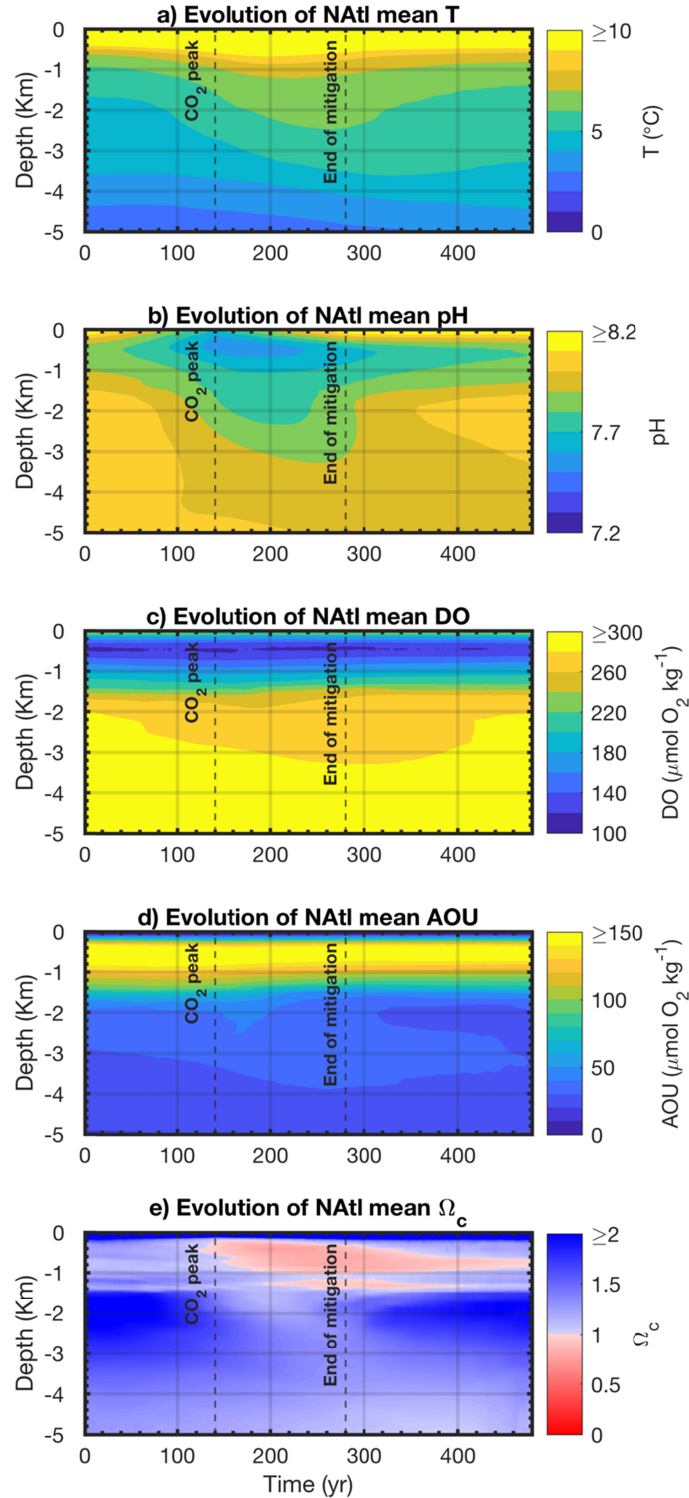
337 remained as low as  $100 \mu\text{mol kg}^{-1}$ . Deep ventilation at the base of the mesopelagic NATl is  
338 compromised during the Ramp-up, with a sustained signal of deoxygenation at depths  
339  $>2000$  m. However, when it comes to depths between 1500 m and 2000 m, it is evident that  
340 after model year 180 there is an oxygenation trend (Fig. 2c), with an apparent shallowing of  
341 oxygen isolines (see discussion).

342

343 The evolution of the mean AOU vertical profile up to model year 200 shows a relative  
344 increase in the deep NATl (between 2000 m and 4000 m) when compared to PI levels. From  
345 model year 200, however, our results indicate a decrease in AOU at depths between 1000 m  
346 and 2000 m, which is linked to the enhanced ventilation associated with a rebound of AMOC  
347 strength (oxygenation is also detected in the same period). From model year 300, AOU  
348 levels in the deeper mesopelagic NATl (roughly at 2000 m deep) reach their lowest values  
349 (Fig. 2d).

350

351 The evolution of the mean  $\Omega_c$  vertical profile shows that the deep ocean calcite lysocline  
352 reaches its shallowest position during model year 140, coinciding with the peak of  $\text{CO}_{2\text{atm}}$   
353 (Fig. 2e). In the upper mesopelagic (between 500 m and 1000 m), conditions favouring  
354 calcite dissolution start to arise from model year 120 and persist throughout the duration of  
355 the simulation. In the middle of the mesopelagic (1500 m deep), conditions favouring calcite  
356 dissolution arise  $\sim 80$  years later and persist until model year 400.



357

358 Figure 2 – Temporal evolution of mean vertical profiles of volume-weighted **a)** Temperature (T), **b)**  
 359 pH, **c)** Dissolved Oxygen (DO), **d)** Apparent Oxygen Utilization (AOU) and **e)** Calcite saturation state  
 360 ( $\Omega_c$ ) throughout the simulation for the North Atlantic. Dashed vertical lines mark model year 140, when  
 361  $\text{CO}_{2\text{atm}}$  reaches its peak in the atmosphere (1135.16 ppm) and model year 280, when the mitigation  
 362 trend stopped and  $\text{CO}_{2\text{atm}}$  returned to the PI baseline (284.7 ppm).

### 363 3.2 Temperature (T)

364  
365 The vertical profile based on an envelope of 2PIsd suggests that the mean ToD for  
366 Temperature in the upper NATl is highly delayed (Fig. 3a), with moderate values of ToD  
367 ( $60\pm 10$  yr) in the first 50 m of the water column, followed by a zone of climate change  
368 buffering down to 200 m deep encompassing the highly variable thermocline, marked by  
369 the highest ToD ( $85\pm 40$  yr). Below the thermocline, Temperature ToD decreases  
370 throughout the mesopelagic NATl with values of  $40\pm 10$  yr.

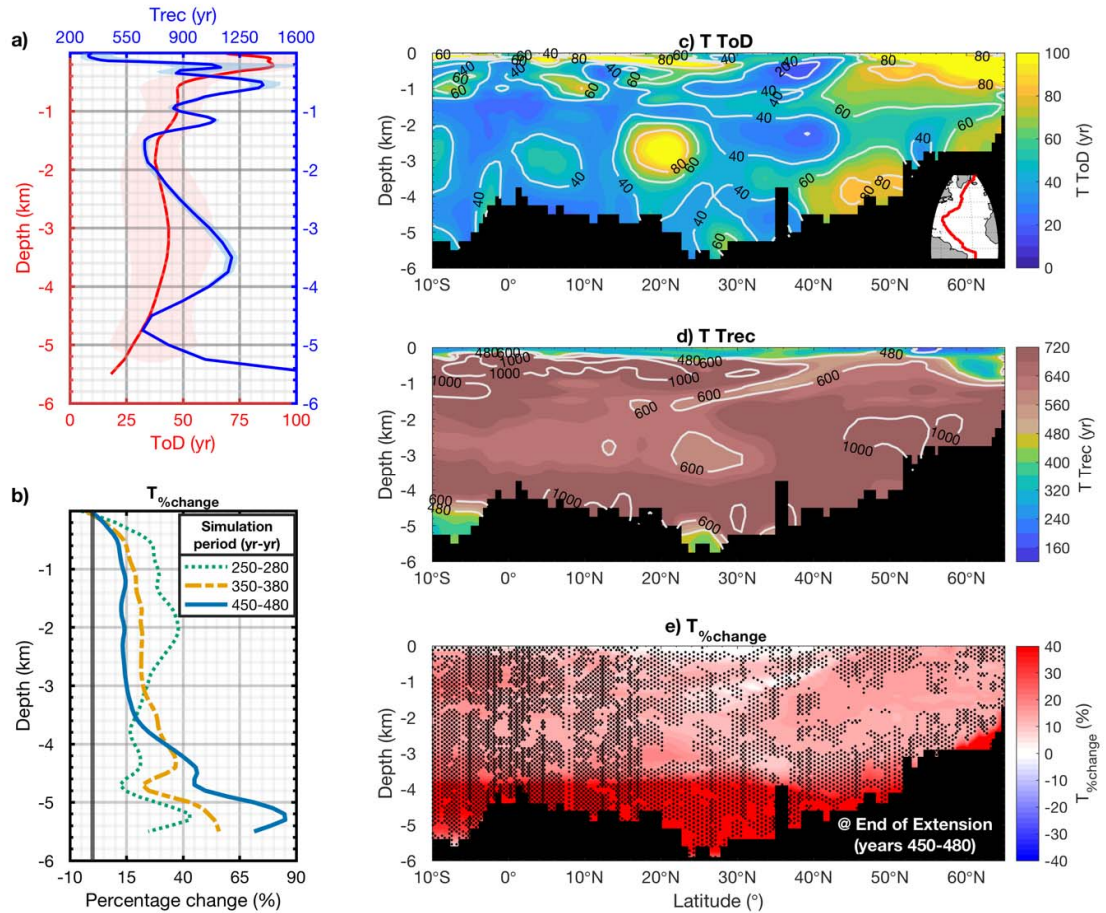
371  
372 The meridional section along the western NATl shows relatively later departures in the  
373 mesopelagic north of  $40^\circ\text{N}$  (Fig. 3c). South of  $40^\circ\text{N}$ , ToD values decrease throughout the  
374 mesopelagic, indicating domains that are more sensitive to climate change with respect  
375 to fluctuations in Temperature. Time of recovery ( $T_{\text{rec}}$ ) estimates show virtually no  
376 recovery within the time span of the simulation, with projected values no lower than 700  
377 years occurring throughout most parts of the NATl section (Fig. 3d). The exceptions were  
378 the very bottom (4500-5000 m), with  $T_{\text{rec}}$  ranging between 300-450 years and the very  
379 surface ( $< 200$  m), where  $T_{\text{rec}}$  values ranged between 320-400 model years. At the very  
380 surface between  $45^\circ\text{N}$  and  $50^\circ\text{N}$ , a patch of low  $T_{\text{rec}}$  values ( $< 200$  years) is simulated.  
381 This marks a region where a cooling trend has been detected (not shown). In this patch,  
382 temperatures up to 10% cooler are projected at the end of the Extension phase, with its  
383 position varying eastwards at depth (see Fig. S3). This feature is also present in other  
384 models [Drijfhout et al., 2012], referred to as the Warming Hole (WH) (see discussion).

385  
386 The model projects NATl interior to be 15% warmer basin-wide, even after mitigating  
387 emissions and allowing for 200 years of extension time (Fig. 3b blue solid line). The top  
388 3000 m of the water column warmed up by up to +40% after the Mitigation phase,  
389 gradually decreasing to +25% and then +15%, from simulation periods 250-280, 350-380  
390 and 450-480 (Fig. 3b dashed green, dashed yellow and solid blue lines, respectively),

391 showing a tendency towards recovery. On the other hand, the delayed response in the  
392 deep NATl is evident at depths greater than 3000 m, where a gradual increase in the  
393 percentage change signal is observed from simulation period 250-280 to 450-480 (Fig.3b  
394 solid blue line reaching values of up more than 50% warmer in the deep NATl). When  
395 looking at the vertical section at the end of the Extension phase (Fig. 3e), our results  
396 suggest significant changes of up to 20% and 50% warmer in the mesopelagic and deep  
397 Natl, respectively.

398

399 It is important to highlight that the warming signal seems to be stronger in low-latitude  
400 regions, suggesting unlikely recoveries in the deepest domains (>3000 m deep).  
401 Conversely, there is a gap in terms of significant differences in the lower mesopelagic  
402 (1000-3000 m deep; Fig. 3e) between 40°N and 60°N, which suggests eventual  
403 recoveries in this zone outside the timeframe of our simulations.



404  
 405  
 406  
 407  
 408  
 409  
 410  
 411  
 412  
 413  
 414  
 415  
 416  
 417

Figure 3 - North Atlantic (0-65°N) volume-weighted vertical profiles of **a**) mean Temperature ToD and Trec (yr), solid red and blue lines respectively and **b**) mean Temperature percentage change (%), across different simulation periods: years 250-280 (end of Mitigation phase), years 350-380 (halfway through the Extension phase) and years 350-380 (end of Extension phase); panels **c-e** show the meridional section along the western side of the basin (red line in panel c, bottom right corner) of temperature **c**) ToD, **d**) Trec, with brown-shaded areas indicating recovery outside the time span of the simulation (> 480 yr), and **e**) percentage change (%) at the end of Extension phase. Stippling in **(e)** indicates regions of significant differences relative to the PI values. Units in **(a, c, d)** are model years since the start of the simulation. Shading around solid lines in panel **(a)** represent uncertainty range estimated using different natural variability envelopes (see Sect. 2.4).

418

419

### 3.3 Dissolved Oxygen (DO)

420

421

ToD for Dissolved Oxygen (DO, Fig. 4a) and AOU (see Fig. S4) indicate an overall consistent and decreasing pattern with narrowing uncertainties at depth until the base of the mesopelagic (2000 m). Subsurface DO and AOU ToD estimates show values of  $100 \pm 30$  yr, whereas at 2000 m deep values are  $\sim 45 \pm 15$  yr. The narrowing of the DO ToD spread reflects the relatively stable mesopelagic NATl with respect temporal fluctuations in DO. Additionally, a feature of particularly high DO ToD values is observed at 2000-3000 m depths in 20-30°N (Fig. 4c), suggesting a highly delayed anthropogenic signal which matches the pattern observed in Fig. 3a for Temperature. These delays indicate the relatively weak influence of the NADW water mass in this region.

430

431

Trec timescales for DO increase gradually from the subsurface towards a local maximum in the mesopelagic NATl, followed by a decrease down to 3000 m and a subsequent increase towards the deep ocean (Fig. 4a). In the subsurface down to the upper mesopelagic (1000 m), recoveries are projected to occur within the time span of our simulation ( $T_{rec} < 480$  years) except for two domains at the subsurface comprised between 5-10°N and 20-30°N where projected timescales of Trec seem to be at least twice as long (Fig. 4d).

438

439

In the mesopelagic NATl between 2000-3000 m deep, recoveries are projected to occur no less than 1300 model years after the start of the Anthropogenic simulation, with two particularly high-Trec clusters, one in the equatorial region between 0-5°N and another in the subarctic domain between 50-60°N (Fig. 4d). Past 3000 m deep, the subsequent decrease in Trec is associated with likely recoveries within the time span of the simulation between 40-60°N, suggesting that the AMOC is regaining its strength and the recovery of DO towards PI levels is initiated. Overall, our results indicate that both the subsurface and the very deep domains are likely to recover before the mesopelagic

446

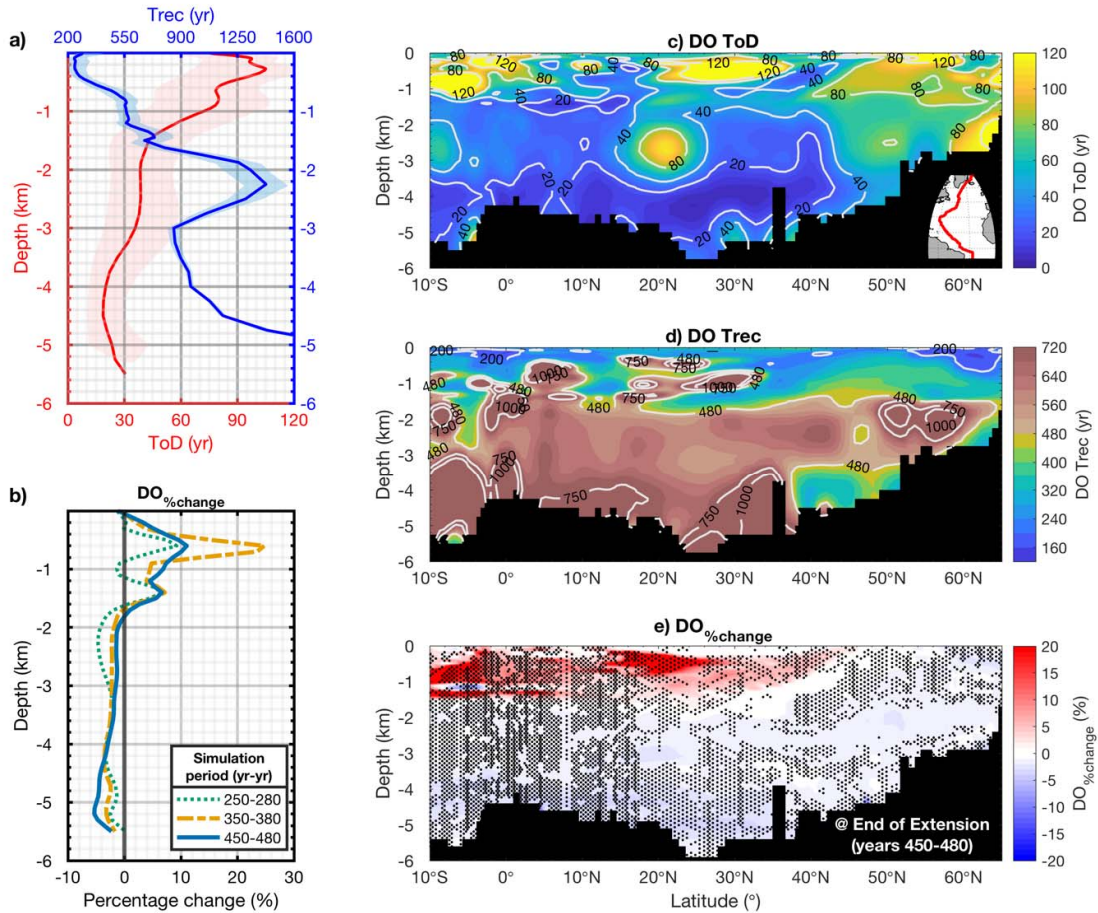
447 domain, where a tongue of particularly high DO Trec values persists between 1000-  
448 3000 m.

449

450 Our results for DO percentage change show two contrasting domains (Fig. 4b and 4e).  
451 Regions below the NATl mixed layer (i.e., 500-1000 m) experience an oxygenation trend  
452 of +10%, +25% and then returning to +10% relative to the PI levels from the end of  
453 Mitigation to middle of the Extension and end of Extension phases respectively. On the  
454 other hand, the mesopelagic and deep NATl domains experience overall deoxygenation  
455 trends. The mesopelagic between 1500-2000 m is the region with the lowest DO  
456 content, decreasing by 5% at the end of Mitigation phase and regaining DO as the  
457 simulation evolved towards the end of Extension phase, where levels were ~2% lower  
458 than PI values. Conversely, the delayed response in the deep NATl is apparent from the  
459 subsequent decreases in DO, with the highest DO change (-6%) at the end of the  
460 simulation.

461

462 It is important to highlight that the oxygenation just below the mixed layer is limited to  
463 the region south of 30°N. North of 30°N, a slight but significant trend of deoxygenation is  
464 simulated (Fig. 4e). Additionally, the gap in terms of significant differences in the  
465 mesopelagic NATl (1000-3000 m) between 40°N and 60°N suggests eventual recoveries  
466 in this zone outside the timeframe of our simulation similar to the pattern for  
467 Temperature (Fig. 3e).



468  
 469 Figure 4 - North Atlantic (0-65°N) volume-weighted vertical profiles of **a**) mean DO ToD and Trec (yr),  
 470 solid red and blue lines respectively and **b**) mean DO percentage change (%), across different  
 471 simulation periods: years 250-280 (end of Mitigation phase), years 350-380 (halfway through the  
 472 Extension phase) and years 350-380 (end of Extension phase); panels **c-e** show the meridional  
 473 section along the western side of the basin (red line in panel c, bottom right corner) of DO **c**) ToD, **d**)  
 474 Trec, with brown-shaded areas indicating recovery outside the time span of the simulation (> 480 yr),  
 475 and **e**) percentage change (%) at the end of Extension phase. Stippling in **(e)** indicates regions of  
 476 significant differences relative to the PI values. Units in **(a, c, d)** are model years since the start of the  
 477 simulation. Shading around solid lines in panel **(a)** represent uncertainty range estimated using  
 478 different natural variability envelopes (see Sect. 2.4).  
 479

### 480 **3.4 Calcite Saturation State ( $\Omega_c$ )**

481  
482 The onset of climate change for  $\Omega_c$  can be detected throughout the water column in less  
483 than 50 years (Fig. 5a,c), correlating tightly with patterns from the pH ToD profile (see  
484 Fig. S5). The subsurface zone (0-500 m) shows the earliest departures ( $10\pm 5$  yr) due to  
485 the decrease in pH as a result of enhanced  $\text{CO}_2$  uptake from the atmosphere. In the  
486 upper mesopelagic (500-1500 m deep) a relatively higher  $\Omega_c$  ToD is simulated ( $50\pm 15$   
487 yr), forming a buffer zone for ocean acidification. This part of the NATl is mainly  
488 influenced by two major clusters of relatively high ToD values, between  $15\text{-}30^\circ\text{N}$  at  
489  $\sim 1000$  m and between  $45\text{-}60^\circ\text{N}$  at 1500 m (Fig. 5c).  $\Omega_c$  ToD decreases gradually  
490 between 1500-3000 m, reaching practically homogeneous values within the 2500-3500  
491 m depth range that are similar to that found at the very surface ( $10\pm 5$  yr). This shows not  
492 only the connectivity of this zone via deep ocean ventilation but also a very stable  
493 environment that is prone to change. In the deepest part of NATl, the results from our  
494 simulation show a gradual increase in  $\Omega_c$  ToD values.

495  
496 Lower  $\Omega_c$  Trec values (up to 320 years), were characteristic of the surface, between 0  
497 and 250 m deep, and throughout the mesopelagic north of  $35^\circ\text{N}$  down to 2500 m depth  
498 (Fig. 5a, d). This shows that recoveries with respect to  $\Omega_c$  are unlikely during the  
499 simulated Mitigation phase and are only observed some 50 years into the Extension  
500 phase. Conversely, south of  $35^\circ\text{N}$ , relatively late Trec values were obtained for most of  
501 the subsurface, mesopelagic and deep NATl domains with estimates no lower than 500  
502 years and even higher southwards (Fig. 5d). It is important to highlight the presence of a  
503 particularly high  $\Omega_c$  Trec region observed between 2000-3000 m deep around  $20^\circ\text{N}$ ,  
504 where Trec are greater than 1000 years. This region coincides with the zone of relatively  
505 early departures of  $\Omega_c$  and to zones of delayed departures of DO and T.

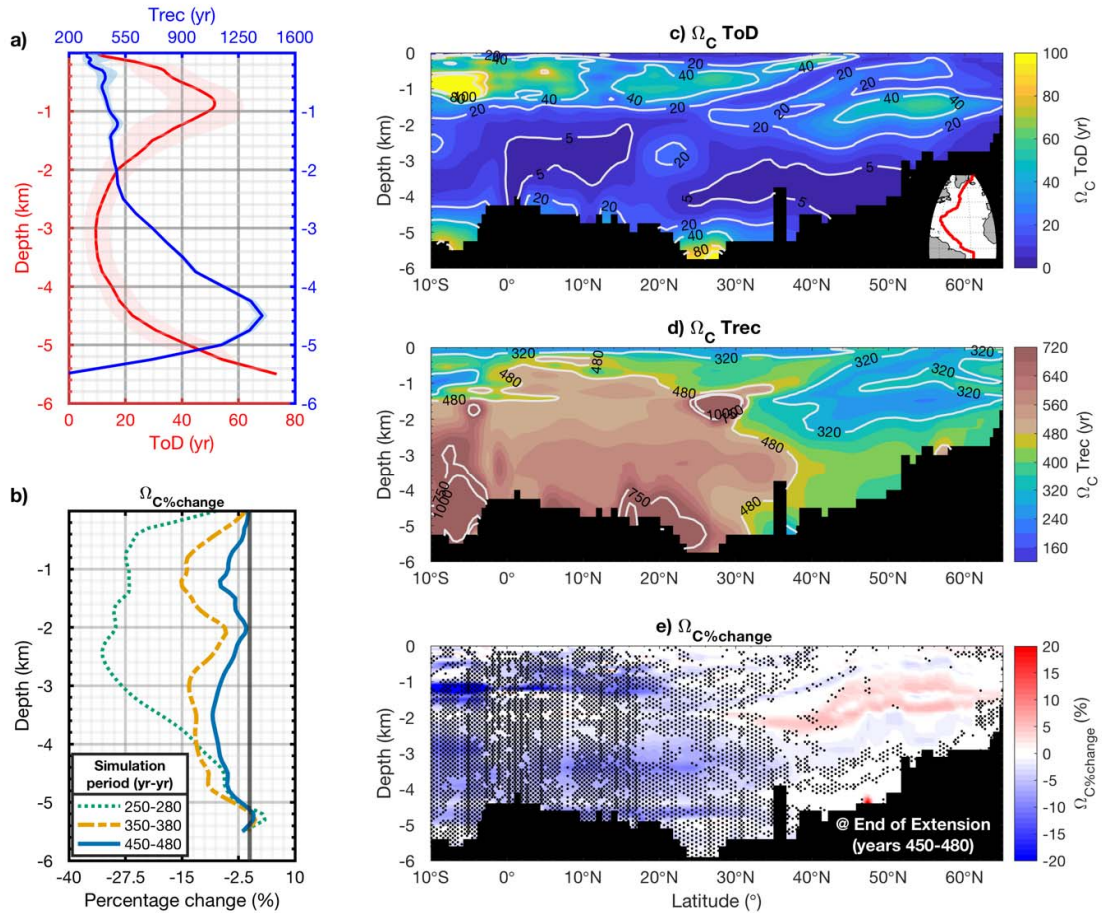
506  
507 Figure 5b shows that the period with the highest percentage change of  $\Omega_c$  in the NATl is  
508 at the end of the Mitigation phase, where saturation states decreased by more than 25%

509 in the entire mesopelagic (1000-3000 m) relative to PI levels. These negative changes  
510 are attenuated over time, with absolute negative changes decreasing from approximately  
511 15% to <5% from the middle to the end of the Mitigation phase, respectively.

512

513 When looking at the last 30 model years, a significant portion of the NATl north of 30°N is  
514 characterized by 0% change suggesting likely recoveries, both in the subsurface and at  
515 2000 m depth (Fig. 5e). However, some regions encompassed by the meridional section  
516 show an overall significant decrease of up to -10% even at the end of the Extension  
517 phase south of 20°N, with a localized minimum of up to -20% at around 1000 m.  
518 Furthermore, north of 30°N, a small tendency towards increased calcite saturation states  
519 is simulated (up to +5%) and associated with insignificant differences between 1000-  
520 2000 m, which suggests an overall recovery followed by a minor  $\Omega_c$  overshoot in the  
521 mesopelagic NATl.

522



523

524 Figure 5 - North Atlantic (0-65°N) volume-weighted vertical profiles of **a**) mean  $\Omega_c$  ToD and Trec (yr),  
 525 solid red and blue lines respectively and **b**) mean  $\Omega_c$  percentage change (%), across different  
 526 simulation periods: years 250-280 (end of Mitigation phase), years 350-380 (halfway through the  
 527 Extension phase) and years 350-380 (end of Extension phase); panels **c-e** show the meridional  
 528 section along the western side of the basin (red line in panel c, bottom right corner) of  $\Omega_c$  **c**) ToD, **d**)  
 529 Trec, with brown-shaded areas indicating recovery outside the time span of the simulation (> 480 yr),  
 530 and **e**) percentage change (%) at the end of Extension phase. Stippling in **e**) indicates regions of  
 531 significant differences relative to the PI values. Units in **(a, c, d)** are model years since the start of the  
 532 simulation. Shading around solid lines in panel **(a)** represent uncertainty range estimated using  
 533 different natural variability envelopes (see Sect. 2.4).

534

### 535 **3.5 Export Production (EP)**

536

537 Figure 6a and b shows that an expansion of the low EP area is noticeable in the  
538 subtropical gyre and the western part of the NAtl, over the Sargasso Sea domain.  
539 Conversely, at higher latitudes, there has been an intensification north of 45°N between  
540 40-45°W, which coincides with the latitudes of WH occurrence.

541

542 The simulated EP ToD ranged between 100 and 150 years (Fig. 6c, e), or no departures  
543 at all. The zonally-averaged EP ToD revealed values of relatively early departures  
544 towards the Equator and patches of 'no departure' predominantly throughout the  
545 eastern NAtl between 30-45°N and in higher latitudes (>60°N; Fig. 6e). Late departures  
546 are found in the transition regions between the subtropical and the subpolar gyres (~180  
547 years) and coincide with the regions with the highest natural variability such as the  
548 Labrador Sea and the WH area.

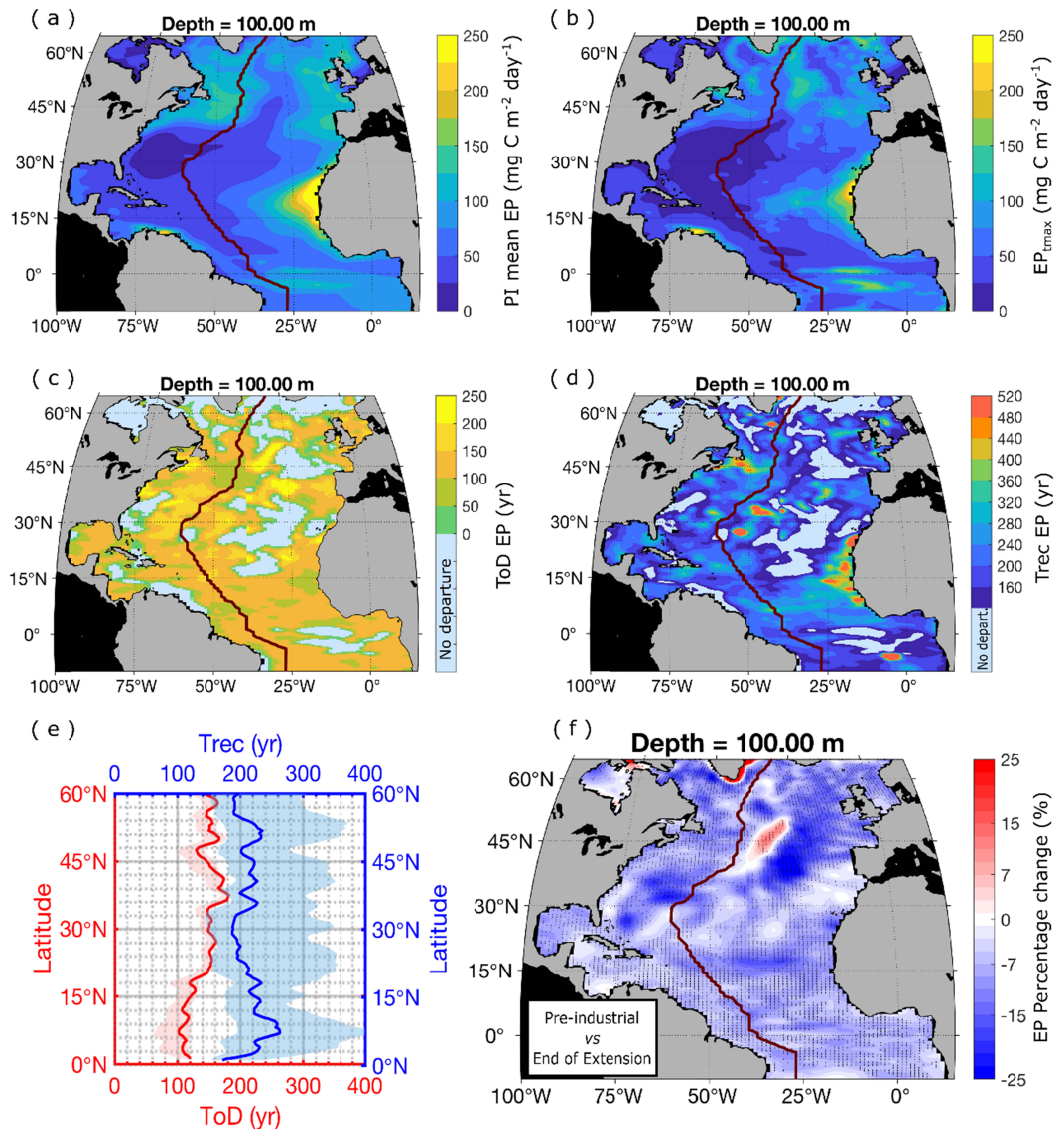
549

550 Overall EP Trec estimates reveal a homogeneous meridional distribution with mean  
551 values of ~200 years, suggesting that recovery timescales are projected to occur  
552 towards the end of the Mitigation phase. A relative increase towards lower latitudes is  
553 projected, but Trec remain lower than 250 years, indicating delayed recoveries in this  
554 region. This is mainly attributed to the high natural envelope simulated both at the  
555 Canary and western African upwelling regions (Fig. 6d). Other exceptions include the  
556 Azores and the Grand Banks off Newfoundland, where Trec were outside of our  
557 simulation period (>480 years).

558

559 Compared to the PI, EP at the end of the Mitigation phase is projected to decrease  
560 between -20% and -25%, except for a region encompassing the western part of the  
561 Irminger Sea and the domain from the Reykjanes Ridge to the Azores, where  
562 percentage change exceeded +25%, coinciding with the WH region (see Fig. S6). Both

563 the positive and the negative changes gradually decrease over time in terms of  
 564 magnitude and spatial extent. At the end of the Extension phase, our results indicated  
 565 that the NATl domain becomes largely less productive with an overall decrease in EP by  
 566 up to -20% in parts of the subtropics. However, positive changes over the Azores ridge  
 567 and the western Irminger Sea remain, with EP values of up to +15% higher than PI,  
 568 showing some localized increase in export production over the WH region (Fig. 6f).



569

570 Figure 6 – Maps of **a)** Pre-industrial mean of Export Production (EP) distribution [ $\text{mg C m}^{-2} \text{ day}^{-1}$ ]; **b)**  
 571 EP at  $t_{\text{max}}$  [ $\text{mg C m}^{-2} \text{ day}^{-1}$ ]; **c)** EP Time of Departure (ToD) and **d)** EP Time of Recovery;  
 572 North Atlantic (0-65°N) zonally-averaged EP ToD and Trec (yr) and **f)** mean EP percentage change (%) at  
 573 the end of Extension phase, where stippling indicates regions of significant differences. The timescale  
 574 estimates are based on an envelope of 2 standard deviations with light blue areas showing regions of  
 575 no departure in panels (c) and d). All year units are model years since the start of the simulation.

576 Shading around solid lines in panel (e) represent uncertainty range estimated using different natural  
577 variability envelopes (see Sect. 2.4).

#### 4. Summary and Discussion

##### Temperature (T)

The delayed climate change onset (ToD) in the shallow NATl (Fig. 3a) and, more specifically, at latitudes between 10-30°N and poleward of 50°N (Fig. 3c), indicates respectively not only subsurface water isolation in the NATl subtropics but also that the anthropogenic signal is relatively smaller when compared to the natural variability of Temperature, especially at temperate and subarctic latitudes, highlighting the tight coupling between atmospheric variability, heat exchange and the gyre circulation. Additionally, our simulation yields maximum ToD within the thermocline zone (Fig. 3a, c), suggesting that this region can be understood as a buffer zone in terms of seawater warming. Here, a sustained long-term anthropogenic perturbation more than in any other region is needed before an evident climate change signal can be detected. A recent study by *Hameau et al.* [2019] focused on changes within the thermocline (200-600 m) under RCP 8.5 (Representative Concentration Pathways) future scenario also suggests delayed ToD for temperature around ~20°N by the end of the century within the thermocline domain, which is consistent with our results and suggests a climate change buffer zone influenced either by high natural variability or inhibited anthropogenic response or even a combination of both as also suggested in the *Hameau et al.* [2019] study. This highlights the need of further studies to better understand the biogeochemical feedbacks in the thermocline domains as well as the mixed layer under strong anthropogenic forcing.

In contrast, despite delays in temperature ToD at the domains described above, our results suggest that changes in the interior NATl can occur as early as 40 years in our scenario of rapid atmospheric warming. Past the thermocline, the uniformly lower ToD values (Fig. 3a,c) indicate how sensitive the mesopelagic and deep NATl zones are and how early global warming can have an impact on their ecosystems relative to the surface

607 and subsurface layers. Furthermore, our results show that the narrowest ToD spread is  
608 simulated in the mesopelagic zone, highlighting its stable environmental condition and,  
609 consequently, its susceptibility to fluctuations in T compared to other regions of the NATl  
610 interior.

611

612 The projected low Trec at both the deepest domains of the NATl (4500-5000 m) and the  
613 superficial layer (<200 m) suggest that the former can be attributed to a thermohaline  
614 recovery signal brought by the AABW and the latter to a recovery in subsurface levels  
615 due to the atmospheric readjustment and recovery (cooling) signals propagating quickly  
616 from the surface to the subsurface levels (Fig. 3a).

617

618 For most of the NATl domains, the persistence of the warming signal is an indicative of  
619 very slow recoveries within the time span of our simulation towards PI levels (Fig. 3e).  
620 We highlight that changes occurring in the South Atlantic and the Southern Ocean are  
621 potentially more pronounced and can play a key role in the redistribution of heat and its  
622 exchange at intermediate layers of the NATl once the AMOC regains its strength.

623

#### 624 **Dissolved Oxygen (DO)**

625

626 Our results indicate an overall deoxygenation in the upper layers of the NATl throughout  
627 the Ramp-up, with greater ToD values than in the deeper layers, which reflect the wider  
628 envelopes associated with the high interannual variability within the mixed layer. Our  
629 results are consistent with those from *Hameau et al.* [2019] (Fig. 2a therein), who also  
630 suggest relatively higher ToD timescales for oxygen in shallower domains of the interior  
631 NATl (<600 m), except for the regions between the centre of the subtropical gyre and the  
632 western side of the basin, where the emergence of anthropogenic signal is early due to  
633 the strong influence of the upper MOW.

634

635 Towards the deep NATl interior, the simulated ToD values decrease, indicating the  
636 stable mesopelagic environment with respect to DO. Interestingly, departures within the  
637 upper layers were generally associated with a deoxygenation whereas for the upper  
638 mesopelagic between 500-2000 m this was not the case.

639

640 Our results show that departures can also be associated with an increase in DO that is  
641 closely linked to reduced AOU at depth. The relationship between an AOU undershoot  
642 and a DO overshoot is evident when analysing: 1) the profiles of DO and AOU Trec,  
643 where a peak of delayed Trec in AOU (between 700-1500 m) is lying just above the  
644 peak of delayed Trec for DO (between 1800-2400 m) (Fig. S7) and 2) the mean DO and  
645 AOU percentage change profiles across all the different simulation periods from the  
646 subsurface down to 2000 m (Fig. 4b and Fig. S4b), which clearly show sustained  
647 positive (negative) changes for DO (AOU). The magnitude of these changes for DO  
648 decreases chronologically after model year 250, meaning a rebound of ventilation in the  
649 upper 2000 m, whereas the magnitude of AOU percentage change did not show a trend  
650 towards PI levels and remained at constant negative values.

651

652 The combination of a DO overshoot and a constant AOU undershoot between 1000-  
653 2000 m deep after mitigation indicates that the oxygen build-up in the mesopelagic NATl  
654 is likely a result of less oxygen utilization over time, a feature also found in other studies  
655 [Tjiputra *et al.*, 2018]. At the WH, more specifically, observational data at intermediate  
656 depths (~1200m) already show a weak oxygenation trend in this domain of the NATl  
657 [Oschlies *et al.*, 2018]. Overall, our simulation suggests that this effect is a direct  
658 consequence of reduced EP from the surface layers to the NATl interior (Fig. 6f), which  
659 creates a surplus of unutilized oxygen at depth when compared to the PI.

660

661 Another feature to highlight is the relatively high delay in terms of DO (and T) ToD, from  
662 2000-3000 m and between 20-30°N. This is likely associated with shifts in the depth

663 horizon of central water masses far west in the interior NATl (Fig. 4c). Under a rapid  
664 anthropogenic warming, the NorESM1-ME tends to produce deeper formation zones for  
665 central water masses, such as the Western North Atlantic Central Water (WNACW),  
666 which receives input from the Mediterranean Overflow Water (MOW). *Liu and Tanhua*  
667 [2019] described that the WNACW normally occurs in the upper layer down to 1000 m.  
668 This is consistent with our results (Fig. 2), where isolines of T and DO in the interior NATl  
669 shifted down by more than 1000 m, yielding a new depth level of ~2000 m. Additionally,  
670 by analysing both the Ttmax and DOtmax surfaces within the 500-2500 depth range  
671 against the model years in which these signals are observed (Figs. S8 and S9  
672 respectively), it is demonstrated that this particular domain is largely influenced by  
673 warming that originates in the Mediterranean Sea.

674

675 In the phase comprising the last 30 model years of the simulation (Fig. 4e), most  
676 domains of the NATl interior north of 40°N tend to show minor deoxygenation trends (up  
677 to -5% compared to PI levels), whereas south of 40°N in the upper mesopelagic there  
678 are still domains where significantly strong oxygenation trends of +20% can be seen,  
679 with the opposite trend in AOU for the same domain (Fig. S4e). Furthermore, the depth  
680 range of these domains increases southwards, reflecting the strong effect of  
681 remineralization rates in low and mid-latitude upper ocean water masses of the South  
682 Atlantic on DO levels of the interior NATl, namely Antarctic Intermediate Water (AAIW).  
683 This shows that, under our simulation, the NorESM1-ME yields recoveries timescales  
684 for the South Atlantic that are significantly longer when compared to the NATl,  
685 highlighting that DO recoveries in the low to mid-latitude domains of interior NATl also  
686 rely on the readjustment timescales of water masses from the South Atlantic.

687

688 Between 2000-3000 m, while the AOU signal shows overall recoveries towards PI levels  
689 in the NATl within our simulation period (Fig. S4d), DO levels show no recovery (Fig. 4d).  
690 This indicates that, even though there was a recovery with respect to the amount of

691 oxygen being consumed for remineralization, the major factor impeding DO recovery  
692 within this depth range is the solubility effect of T prevailing in the South Atlantic, which  
693 reduces DO levels at depth even after the Extension phase (Fig. 4b and 4e).

694  
695  
696  
697  
698

### **Calcite Saturation State ( $\Omega_c$ )**

698 The basin-scale evolution of  $\Omega_c$  (Fig. 2e) shows that conditions favouring calcite  
699 dissolution start to arise just before the  $\text{CO}_{2\text{atm}}$  peak in the Ramp-up phase (model year  
700 120). Our results suggest that, under strong anthropogenic forcing, the whole NATl  
701 experienced conditions very close to the dissolution horizon for as long as 150 years,  
702 encompassing the whole Mitigation phase (model years 140-280). This highlights the  
703 time lag between the implementation of mitigation measures and the actual response in  
704 the interior ocean.

705

706 The ToD timescales along the meridional section revealed domains of delayed  
707 departures both in the upper mesopelagic (~1000 m) and the deep ocean domains  
708 south of 30°N. These delayed departures seem to be a result of volume input from the  
709 South Atlantic, particularly due to the enhanced contribution of Antarctic Intermediate  
710 Water (AAIW) in the upper mesopelagic domain and AABW in the deep ocean, which  
711 are characterized by relatively high pH compared to already-affected NADW domain  
712 (Fig. S5c). The AAIW penetrates the NATl mesopelagic up to ~40°N, delaying low-pH  
713 water mass penetration despite the abrupt drop in pH induced by strong atmospheric  
714 exchange at latitudes > 50°N. This indicates that one of the major processes controlling  
715 the decrease and the spread of the low  $\Omega_c$  signal in the upper mesopelagic NATl is the  
716 interplay between northward transports from the South Atlantic and the time when the  
717 AMOC slows down at subduction zones. This gradual change towards a weaker AMOC  
718 creates some latency which allows for a short-lived dominant buffering effect with  
719 respect to the penetration of a relatively high pH signal from the south. Our results also

720 suggest that the buffering effect of AABW is less predominant if compared to the effect  
721 of AAIW in the mesopelagic. Understanding this latent relationship along with the  
722 opposing transport effects occurring at intermediate depths is crucial to projecting more  
723 precisely not only the contributions of unaltered volumes from the South Atlantic, which  
724 in turn are able to curb the low-acidity signal brought by NADW, but also improve the  
725 estimates of ToD timescales. We highlight that this dynamical feature could be model  
726 dependent and future analysis using different model systems would be valuable.

727

728 Overall, decreases in  $\Omega_c$  peaked at the end of Mitigation (model years 250-280), with the  
729 volume-weighted profile for the whole NATl from 0-65°N (Fig. 5b) showing saturation  
730 states 25% lower than PI levels for the entire mesopelagic (1000-3000 m). Furthermore,  
731  $\Omega_c$  undersaturation persists throughout the whole simulation in the upper mesopelagic  
732 between 500-1500 m (Fig. 2e), meaning unlikely recoveries in that zone even after the  
733 Extension phase. However, when the extent of recovery along the meridional section is  
734 examined, a distinct separation is seen at the latitude of 35°N. Most domains in the  
735 interior NATl north of 35°N showed recoveries within the last 30 years of the simulation  
736 and even some minor  $\Omega_c$  overshoots between 1000-2000 m, likely linked to the re-  
737 introduction of relatively high-pH water masses from other regions. Conversely, south of  
738 35°N significant undershoots are still present and are pronounced in domains that are  
739 influenced by intermediate and deep water masses from the South Atlantic, such as  
740 AAIW (~1000 m) and AABW (>3500 m) respectively. This indicates that the  
741 anthropogenic disturbance is still propagating within the South Atlantic as a persisting  
742 decrease in pH which is reflected in the  $\Omega_c$  signal in the NATl interior (Fig. S5e).

743

744 Unlike what has been observed for the departure timescales associated with T and DO,  
745 ToD values for  $\Omega_c$  did not form a cluster of delayed departures in the domain  
746 characterized by the influence of the MOW (Fig. 5b, ~30°N). This shows that

747 anthropogenic disturbances altering the  $\Omega_c$  signal in the Mediterranean are readily  
748 cascading through the mid-latitude zones of central water masses in the NATl.  
749 Interestingly, while a cluster of delayed recoveries cannot be observed for T at the  
750 domain dominated by intermediate-depth water masses, as late recoveries seem to be  
751 widespread over the interior NATl, our results revealed the presence MOW-related  
752 clusters of delayed Trec for both DO and  $\Omega_c$  (Fig. 4d and 5d). However, their depth  
753 range differs, with the DO cluster appearing at a shallower position (~1000 m) when  
754 compared with that of  $\Omega_c$  ~1500 m. This disparity in depth horizon can partially be due to  
755 changes in biological activity and a consequence of enhanced EP (see below), which  
756 initially induces high remineralization at intermediate levels and causes a subsequent  
757 injection of DIC at deeper levels, therefore decreasing overall pH and sustaining a net  
758 decrease in  $\Omega_c$ .

759  
760  
761

### **Export Production (EP)**

762  
763

Our results reveal a generalised spread of low-production zones, especially on the  
764 western side of the NATl subtropical gyre. Eastwards, decreases are also noticeable  
765 when we take into account the contrast between the PI mean and  $EP_{tmax}$  (Fig. 6a and  
766 6b), with widespread decreases along the European shelf (45°N,10°W) as well as a  
767 significant reduction over the Canary upwelling system (22°N,18°W). However, some  
768 patches of localized increase in export production were also observed, especially in  
769 parts of the Irminger Sea and the domain from the Reykjanes Ridge to the Azores,  
770 which are associated with relatively later ToD values (>250 model years, Fig. 6c).

771

772 There is little variation in both zonally-averaged EP ToD and Trec, indicating that, at the  
773 domains where departures were observed, significant changes in export production will  
774 occur no later than ~10 years into the Mitigation phase with a general trend towards  
775 earlier departures in higher latitudes (Fig. 6c and 6e).

776

777 The last 30 model years of the simulation reveal a scenario of predominant decrease in  
778 export production except for the WH area in the subpolar region, where trends towards  
779 cooling, oxygenation and increased EP were detected at the end of the simulation. The  
780 increases in DO and EP signals seem to result from enhanced instability in the water  
781 column caused by the decrease in T, which deepens the mixed layer depth (MLD),  
782 favouring productive regimes as well as enhanced ventilation.

783

784

## 785 **5. Conclusion**

786

787

788

789

790

791

792

793

794

795

796

797

798

799

800

801

802

803

804

Despite applying symmetrical forcing (i.e., a CO<sub>2</sub> ramp-up of +1% yr<sup>-1</sup> followed by a CO<sub>2</sub> ramp down -1% yr<sup>-1</sup>), our study reveals that the responses observed in the interior NATl in terms of physical and biogeochemical drivers were asymmetric, with strong spatial variations that remained even after allowing for stabilization over the Extension phase. Our study highlights that vast regions in the interior NATl, especially the mesopelagic, tend to respond to anthropogenic forcing significantly earlier than domains in the subsurface. It is also in these regions of early departure that recovery timescales are most affected, meaning that in regions of relatively rapid change the recovery is even slower. When looking at individual parameters, Temperature data revealed overall unlikely recoveries in the interior NATl towards PI levels. At the end of the experiment, mesopelagic regions displayed modest cooling in response to decreased anthropogenic forcing but remained 15% warmer than the PI on average. Conversely, instead of cooling, our data suggests that Temperature in domains of the deep NATl were progressively warm throughout all the simulation phases. This suggests that domains in the South Atlantic and Southern Ocean accumulated heat as the AMOC slowed down over the Ramp-up. Once the AMOC regained some of its strength, this heat surplus started to be exchanged across the Atlantic, consequently affecting readjustment timescales over the entire deep NATl as far as 50°N.

805

806 With respect to oxygen, our data suggests a pattern of rather counterintuitive  
807 oxygenation despite the anthropogenic warming in the mesopelagic NATl. This oxygen  
808 overshoot is linked to a decrease in biological remineralization, which is caused by a  
809 decrease in export production from the surface layers. This ultimately translates into a  
810 reduction in the organic matter exported to the interior, creating a surplus of unutilized  
811 oxygen relative to the PI. Regarding  $\Omega_c$ , our simulation suggests that departure  
812 timescales in the upper mesopelagic NATl are closely linked to changes in pH and  
813 mediated by the northward transports from the South Atlantic and the gradual  
814 attenuation of the AMOC. This interplay allows for a short-lived dominant buffering with  
815 respect to the penetration of a relatively high-pH signal from the south at intermediate  
816 depths. This buffering effect, however, seems to be stronger in the domains influenced  
817 by AAIW when compared to the domain of the AABW. Further investigations on how  
818 these opposing transports, which counteract the acidity signal from NADW, affect  
819 timescales of climate change are crucial to improve our understanding of how relatively  
820 unaltered volumes from the South Atlantic have an impact on ToD timescales in the  
821 mesopelagic NATl. We emphasize that this dynamical interplay could be a model-  
822 dependent feature and further studies using different models would be valuable.

823

824 Here we show that, for variables which revealed likely recoveries within the timeframe of  
825 the simulation, recovery timescales in the NATl interior are out of phase (i.e., not  
826 concurrent). For example, the layered structure of delayed Trec values for DO and  $\Omega_c$  at  
827 mid latitudes reveals that different recovery signals are associated with a Mediterranean  
828 Overflow that is not biogeochemically homogeneous and, thus, an indicative of out-of-  
829 phase recoveries occurring at different domains within the Mediterranean Sea.  
830 Additionally, our results indicate that both the Mediterranean overflow as well as other  
831 intermediate-depth processes regulating water mass restructuring are key in controlling  
832 the recovery of calcite saturation in mid-latitudes of the mesopelagic NATl. Further

833 studies focused on the impacts of biogeochemical shifts not only in the Mediterranean  
834 Overflow but also other important processes that form mid-latitude water masses are  
835 needed to better understand the impacts on the biogeochemistry of the mesopelagic  
836 North Atlantic under climate change.

837

838 Improving how export production is represented in the models is valuable to understand  
839 whether the features observed here arise from adopting a relatively shallow layer, where  
840 productivity is confined to the first 100 m and the recycling of organic matter is not  
841 mediated by an explicit microbial loop. Furthermore, a more robust representation of the  
842 lower trophic ecosystem processes and the adoption of our method using other ESMs  
843 can improve our understanding of any simulated counterintuitive patterns (e.g. the  
844 oxygen overshoot in the mesopelagic NATl followed by warming and the WH region  
845 characterized by cooling and enhanced EP). Such exercise can help us determine, for  
846 example, whether the oxygen overshoot detected here is a model caveat or an actual  
847 indication of the solubility effect being surpassed by biological activity under extreme  
848 climate change. Moreover, the use of more realistic climate change and mitigation  
849 scenarios in such studies, e.g., SSP5-3.4, can ultimately help shed new light on where  
850 the threshold lies in terms of the amount of change that is necessary for the solubility  
851 effect to become less important in controlling DO levels in the NATl interior.

852

853 We highlight that future studies focused on the relationship between AMOC strength,  
854 changes in ocean biogeochemistry and their effects on ToD and Trec timescales in the  
855 deep ocean are needed to better understand how these properties are linked and how  
856 they translate into exposure horizons beyond which significant changes in marine  
857 assemblages are expected. The existing studies that have modelled timing of climate  
858 change emergence (i.e., ToD) as well as timing of exposure to conditions beyond niche  
859 limits are scarce for marine species, mostly confined to the epipelagic zone and have  
860 focused on changes in terms of temperature. We currently lack more integrative

861 approaches involving the covarying and synergistic effects of biogeochemical variables  
862 on ecosystem function, which can constrain species range and their tolerance to climate  
863 change scenarios even more [Coll *et al.*, 2020; Trisos *et al.*, 2020].

864

865 To conclude, we reiterate that it is time for the community to start focusing not just on  
866 changes to the marine environment in the epipelagic zone given how vast,  
867 biogeochemically active and interconnected the various domains of the deep NATl are.  
868 The results shown here come from a single model and it would be invaluable to test the  
869 robustness of our results using other models. At the time of our study, the CMIP6 model  
870 CDRMIP simulations were not available. Holistic modelling exercises on how covarying  
871 shifts in biogeochemical drivers can be used as proxies for changes in deep-ocean  
872 marine assemblages are key to better inform policy making. Such studies can ultimately  
873 aid in our understanding of how exposure times can affect carbon and nutrient recycling  
874 at depth, water mass restructuring, as well as species distribution and ultimately help  
875 better project the consequences of extreme climate change scenarios for the deep  
876 ocean.

877

## 878 **6. Acknowledgements**

879

880 We would like to acknowledge the Norwegian Research Council funded projects  
881 ORGANIC (Overturning circulation and its implications for global carbon cycle in  
882 coupled model; № 239965) THRESHOLDS (Thresholds for destabilizing thermohaline  
883 circulation and ocean carbon cycling in a warmer world; № 254964), and COLUMBIA  
884 (Constraining the Large Uncertainties in Earth System Model Projections with a Big  
885 Data Approach; № 275268). This study has been carried out as part of the IMBRSea  
886 Erasmus+: Erasmus Mundus Joint Master's Degree (EMJMD) Programme and  
887 supported by an EMJMD Scholarship, under the EU Grant Agreement № 2016-2280.  
888 The NorESM1-ME ramp-up simulation output is publicly available at the CMIP5  
889 repository: <https://esgf-data.dkrz.de/projects/esgf-dkrz/>. Fully coupled ramp-down and

890 extension simulations are long-term archived at the NorStore Research Data Archive

891 and can be accessed under <https://doi.org/10.11582/2018.00011>.

892

893  
894  
895  
896  
897  
898  
899  
900  
901  
902  
903  
904  
905  
906  
907  
908  
909  
910  
911  
912  
913  
914  
915  
916  
917  
918  
919  
920  
921  
922  
923  
924  
925  
926  
927  
928  
929  
930  
931  
932  
933  
934  
935  
936  
937  
938  
939  
940  
941  
942  
943  
944  
945  
946  
947  
948

## 7. References

- Assmann, K., M. Bentsen, C. Heinze, and J. Segschneider (2010), An isopycnic ocean carbon cycle model, *Geoscientific Model Development*, 3, 143-167.
- Baillon, S., J.-F. Hamel, V. E. Wareham, and A. Mercier (2012), Deep cold-water corals as nurseries for fish larvae, *Frontiers in Ecology and the Environment*, 10(7), 351-356.
- Bentsen, M., I. Bethke, J. Debernard, T. Iversen, A. Kirkevåg, Ø. Seland, H. Drange, C. Roelandt, I. Seierstad, and C. Hoose (2013), The Norwegian earth system model, NorESM1-M—Part 1: Description and basic evaluation of the physical climate, *Geosci. Model Dev*, 6(3), 687-720.
- Boucher, O., P. Halloran, E. Burke, M. Doutriaux-Boucher, C. Jones, J. Lowe, M. Ringer, E. Robertson, and P. Wu (2012), Reversibility in an Earth System model in response to CO<sub>2</sub> concentration changes, *Environmental Research Letters*, 7(2), 024013.
- Box, J., X. Fettweis, J. Stroeve, M. Tedesco, D. Hall, and K. Steffen (2012), Greenland ice sheet albedo feedback: thermodynamics and atmospheric drivers, *The Cryosphere*, 6(4), 821-839.
- Buhl-Mortensen, L., S. H. Olafsdottir, P. Buhl-Mortensen, J. M. Burgos, and S. A. Ragnarsson (2015), Distribution of nine cold-water coral species (Scleractinia and Gorgonacea) in the cold temperate North Atlantic: effects of bathymetry and hydrography, *Hydrobiologia*, 759(1), 39-61.
- Caesar, L., S. Rahmstorf, and G. Feulner (2020), On the relationship between Atlantic meridional overturning circulation slowdown and global surface warming, *Environmental Research Letters*, 15(2), 024003.
- Chen, X., and K.-K. Tung (2018), Global surface warming enhanced by weak Atlantic overturning circulation, *Nature*, 559(7714), 387.
- Coll, M., J. Steenbeek, M. G. Pennino, J. Buszowski, K. Kaschner, H. K. Lotze, Y. Rousseau, D. P. Tittensor, C. Walters, and R. A. Watson (2020), Advancing Global Ecological Modeling Capabilities to Simulate Future Trajectories of Change in Marine Ecosystems, *Frontiers in Marine Science*, 7, 741.
- Costello, M. J., M. McCrea, A. Freiwald, T. Lundälv, L. Jonsson, B. J. Bett, T. C. van Weering, H. de Haas, J. M. Roberts, and D. Allen (2005), Role of cold-water *Lophelia pertusa* coral reefs as fish habitat in the NE Atlantic, in *Cold-water corals and ecosystems*, edited, pp. 771-805, Springer.
- Courtney, T. A., et al. (2017), Environmental controls on modern scleractinian coral and reef-scale calcification, *Science Advances*, 3(11), e1701356, doi:10.1126/sciadv.1701356.
- Drijfhout, S., G. J. v. Oldenborgh, and A. Cimadoribus (2012), Is a Decline of AMOC Causing the Warming Hole above the North Atlantic in Observed and Modeled Warming Patterns?, *Journal of Climate*, 25(24), 8373-8379, doi:10.1175/jcli-d-12-00490.1.
- Friedlingstein, P., R. M. Andrew, J. Rogelj, G. P. Peters, J. G. Canadell, R. Knutti, G. Luderer, M. R. Raupach, M. Schaeffer, and D. P. van Vuuren (2014), Persistent growth of CO<sub>2</sub> emissions and implications for reaching climate targets, *Nature geoscience*, 7(10), 709-715.
- Garcia, H., R. Locarnini, T. Boyer, J. Antonov, M. Zweng, O. Baranova, and D. Johnson (2010a), World Ocean Atlas 2009, edited, Volume.
- Garcia, H., R. Locarnini, T. Boyer, J. Antonov, M. Zweng, O. Baranova, and D. Johnson (2010b), World Ocean Atlas 2009, vol. 4, Nutrients (Phosphate, Nitrate, Silicate), edited by: Levitus, S, NOAA Atlas NESDIS, US Gov. Printing Office, Wash., DC, 71.
- Gasser, T., C. Guivarch, K. Tachiiri, C. Jones, and P. Ciais (2015), Negative emissions physically needed to keep global warming below 2 C, *Nature communications*, 6(1), 1-7.
- Gehlen, M., R. Séférian, D. O. Jones, T. Roy, R. Roth, J. Barry, L. Bopp, S. C. Doney, J. P. Dunne, and C. Heinze (2014), Projected pH reductions by 2100 might put deep North Atlantic biodiversity at risk, *Biogeosciences*, 11(23), 6955-6967.
- Goris, N., J. Tjiputra, J. Schwinger, and C. Heinze (2015), Responses of carbon uptake and oceanic pCO<sub>2</sub> to climate change in the North Atlantic: A model study with the Bergen Earth System Model, *Global Biogeochemical Cycles*, 29(10), 1567-1583.
- Guinotte, J. M., J. Orr, S. Cairns, A. Freiwald, L. Morgan, and R. George (2006), Will human-induced changes in seawater chemistry alter the distribution of deep-sea scleractinian corals?, *Frontiers in Ecology and the Environment*, 4(3), 141-146, doi:10.1890/1540-9295(2006)004[0141:Whcisc]2.0.Co;2.
- Hameau, A., J. Mignot, and F. Joos (2019), Assessment of time of emergence of anthropogenic deoxygenation and warming: insights from a CESM simulation from 850 to 2100 CE, *Biogeosciences*, 16, 1755-1780.
- Hebbeln, D., R. d. C. Portilho-Ramos, C. Wienberg, and J. Titschack (2019), The Fate of Cold-Water Corals in a Changing World: A Geological Perspective, *Frontiers in Marine Science*, 6(119), doi:10.3389/fmars.2019.00119.

949 Hennige, S. J., L. C. Wicks, N. A. Kamenos, G. Perna, H. S. Findlay, and J. M. Roberts (2015), Hidden impacts of  
950 ocean acidification to live and dead coral framework, *Proceedings of the Royal Society B: Biological*  
951 *Sciences*, 282(1813), 20150990, doi:doi:10.1098/rspb.2015.0990.

952 Henry, L.-A., J. M. Navas, S. J. Hennige, L. C. Wicks, J. Vad, and J. M. Roberts (2013), Cold-water coral reef  
953 habitats benefit recreationally valuable sharks, *Biological conservation*, 161, 67-70.

954 Henson, S. A., C. Beaulieu, T. Ilyina, J. G. John, M. Long, R. Seferian, J. Tjiputra, and J. L. Sarmiento (2017), Rapid  
955 emergence of climate change in environmental drivers of marine ecosystems, *Nature Communications*, 8,  
956 doi:10.1038/ncomms14682.

957 Hidalgo, M., and H. I. Browman (2019), Developing the knowledge base needed to sustainably manage  
958 mesopelagic resources, edited, Oxford University Press.

959 Hofmann, M., S. Mathesius, E. Kriegler, D. van Vuuren, and H. Schellnhuber (2019), Strong time dependence of  
960 ocean acidification mitigation by atmospheric carbon dioxide removal, *Nature Communications*, 10(1), 1-  
961 10.

962 IPCC, 2019: Summary for Policymakers. In: IPCC Special Report on the Ocean and Cryosphere in a Changing  
963 Climate [H.-O. Pörtner, D.C. Roberts, V. Masson-Delmotte, P. Zhai, M. Tignor, E. Poloczanska, K.  
964 Mintenbeck, A. Alegría, M. Nicolai, A. Okem, J. Petzold, B. Rama, N.M. Weyer (eds.)]. In press

965 Irigoien, X., T. A. Klevjer, A. Røstad, U. Martinez, G. Boyra, J. Acuña, A. Bode, F. Echevarria, J. I. González-  
966 Gordillo, and S. Hernandez-Leon (2014), Large mesopelagic fishes biomass and trophic efficiency in the  
967 open ocean, *Nature communications*, 5, 3271.

968 Jones, D. O., A. Yool, C. L. Wei, S. A. Henson, H. A. Ruhl, R. A. Watson, and M. Gehlen (2014), Global reductions  
969 in seafloor biomass in response to climate change, *Global change biology*, 20(6), 1861-1872.

970 Keeling, C. D., S. C. Piper, R. B. Bacastow, M. Wahlen, T. P. Whorf, M. Heimann, and H. A. Meijer (2005),  
971 Atmospheric CO<sub>2</sub> and <sup>13</sup>C Exchange with the Terrestrial Biosphere and Oceans from 1978 to 2000:  
972 Observations and Carbon Cycle Implications, in *A History of Atmospheric CO<sub>2</sub> and Its Effects on Plants,*  
973 *Animals, and Ecosystems*, edited by I. T. Baldwin, et al., pp. 83-113, Springer New York, New York, NY,  
974 doi:10.1007/0-387-27048-5\_5.

975 Keller, F. Joos, and C. Raible (2014), Time of emergence of trends in ocean biogeochemistry, *Biogeosciences*,  
976 11(13), 3647-3659.

977 Keller, D. P., A. Lenton, V. Scott, N. E. Vaughan, N. Bauer, D. Ji, C. D. Jones, B. Kravitz, H. Muri, and K. Zickfeld  
978 (2018), The carbon dioxide removal model intercomparison project (CDRMIP): rationale and experimental  
979 protocol for CMIP6, *Geoscientific Model Development*, 11(3), 1133-1160.

980 Key, R. M., A. Kozyr, C. L. Sabine, K. Lee, R. Wanninkhof, J. L. Bullister, R. A. Feely, F. J. Millero, C. Mordy, and T.  
981 H. Peng (2004), A global ocean carbon climatology: Results from Global Data Analysis Project (GLODAP),  
982 *Global Biogeochem. Cycles*, 18(4).

983 Kirkevåg, A., T. Iversen, Ø. Seland, C. Hoose, J. Kristjánsson, H. Struthers, A. Ekman, S. Ghan, J. Griesfeller, and  
984 E. Nilsson (2012), Aerosol-climate interactions in the Norwegian Earth System Model–NorESM,  
985 *Geoscientific Model Development Discussions*, 5(3), 2599-2685.

986 Kwiatkowski, L., O. Torres, L. Bopp, O. Aumont, M. Chamberlain, J. R. Christian, J. P. Dunne, M. Gehlen, T.  
987 Ilyina, and J. G. John (2020), Twenty-first century ocean warming, acidification, deoxygenation, and  
988 upper-ocean nutrient and primary production decline from CMIP6 model projections, *Biogeosciences*,  
989 17(13), 3439-3470.

990 Levin, L. A., and N. Le Bris (2015), The deep ocean under climate change, *Science*, 350(6262), 766-768,  
991 doi:10.1126/science.aad0126.

992 Liu, M., and T. Tanhua (2019), Distribution of Water Masses in the Atlantic Ocean based on GLODAPv2, *Ocean*  
993 *Science Discussions*, 1-32.

994 Mahowald, N. M., A. R. Baker, G. Bergametti, N. Brooks, R. A. Duce, T. D. Jickells, N. Kubilay, J. M. Prospero,  
995 and I. Tegen (2005), Atmospheric global dust cycle and iron inputs to the ocean, *Global biogeochemical*  
996 *cycles*, 19(4).

997 Maier-Reimer, E. (1993), Geochemical cycles in an ocean general circulation model. Preindustrial tracer  
998 distributions, *Global Biogeochemical Cycles*, 7(3), 645-677.

999 McDougall, T. J., and P. M. Barker (2011), Getting started with TEOS-10 and the Gibbs Seawater (GSW)  
1000 oceanographic toolbox, *SCOR/IAPSO WG*, 127, 1-28.

1001 Meyer, J., and U. Riebesell (2015), Reviews and Syntheses: Responses of coccolithophores to ocean  
1002 acidification: a meta-analysis, *Biogeosciences*, 12(6), 1671-1682, doi:10.5194/bg-12-1671-2015.

1003 Oschlies, A., P. Brandt, L. Stramma, and S. Schmidtko (2018), Drivers and mechanisms of ocean deoxygenation,  
1004 *Nature Geoscience*, 11(7), 467-473.

1005 Puerta, P., C. Johnson, M. Carreiro-Silva, L.-A. Henry, E. Kenchington, T. Morato, G. Kazanidis, J. L. Rueda, J.  
1006 Urra, and S. Ross (2020), Influence of Water Masses on the Biodiversity and Biogeography of Deep-Sea  
1007 Benthic Ecosystems in the North Atlantic, *Frontiers in Marine Science*, 7, 239.

1008 Ramirez-Llodra, E., P. A. Tyler, M. C. Baker, O. A. Bergstad, M. R. Clark, E. Escobar, L. A. Levin, L. Menot, A. A.  
1009 Rowden, and C. R. Smith (2011), Man and the last great wilderness: human impact on the deep sea, *PLoS*  
1010 *one*, 6(8), e22588.

1011 Riebesell, U., et al. (2018), Toxic algal bloom induced by ocean acidification disrupts the pelagic food web,  
1012 *Nature Climate Change*, 8(12), 1082-1086, doi:10.1038/s41558-018-0344-1.

1013 Sarmiento, J. L., and C. Le Quere (1996), Oceanic carbon dioxide uptake in a model of century-scale global  
1014 warming, *Science*, 274(5291), 1346-1350.

1015 Schwinger, J., and J. Tjiputra (2018), Ocean carbon cycle feedbacks under negative emissions, *Geophysical*  
1016 *Research Letters*, 45(10), 5062-5070.

1017 Smeed, D., G. McCarthy, S. Cunningham, E. Frajka-Williams, D. Rayner, W. E. Johns, C. Meinen, M. Baringer, B.  
1018 Moat, and A. Duchez (2014), Observed decline of the Atlantic meridional overturning circulation 2004–  
1019 2012, *Ocean Science*, 10(1), 29-38.

1020 Smith, P., S. J. Davis, F. Creutzig, S. Fuss, J. Minx, B. Gabrielle, E. Kato, R. B. Jackson, A. Cowie, and E. Kriegler  
1021 (2016), Biophysical and economic limits to negative CO<sub>2</sub> emissions, *Nature climate change*, 6(1), 42-50.

1022 Steffen, W., J. Rockström, K. Richardson, T. M. Lenton, C. Folke, D. Liverman, C. P. Summerhayes, A. D.  
1023 Barnosky, S. E. Cornell, and M. Crucifix (2018), Trajectories of the Earth System in the Anthropocene,  
1024 *Proceedings of the National Academy of Sciences*, 115(33), 8252-8259.

1025 Tjiputra, K. Assmann, M. Bentsen, I. Bethke, O. Otterå, C. Sturm, and C. Heinze (2010a), Bergen Earth system  
1026 model (BCM-C): model description and regional climate-carbon cycle feedbacks assessment, *Geoscientific*  
1027 *Model Development*, 3(1), 123-141.

1028 Tjiputra, K. Assmann, and C. Heinze (2010b), Anthropogenic carbon dynamics in the changing ocean, *Ocean*  
1029 *Science*, 6(3), 605.

1030 Tjiputra, N. Goris, S. K. Lauvset, C. Heinze, A. Olsen, J. Schwinger, and R. Steinfeldt (2018), Mechanisms and  
1031 Early Detections of Multidecadal Oxygen Changes in the Interior Subpolar North Atlantic, *Geophysical*  
1032 *Research Letters*, 45(9), 4218-4229, doi:10.1029/2018gl077096.

1033 Tjiputra, C. Roelandt, M. Bentsen, D. M. Lawrence, T. Lorentzen, J. Schwinger, O. Seland, and C. Heinze (2013),  
1034 Evaluation of the carbon cycle components in the Norwegian Earth System Model (NorESM), *Geoscientific*  
1035 *Model Development*, 6(2), 301-325, doi:10.5194/gmd-6-301-2013.

1036 Tokarska, K. B., and K. Zickfeld (2015), The effectiveness of net negative carbon dioxide emissions in reversing  
1037 anthropogenic climate change, *Environmental Research Letters*, 10(9), 094013.

1038 Trisos, C. H., C. Merow, and A. L. Pigot (2020), The projected timing of abrupt ecological disruption from  
1039 climate change, *Nature*, 580(7804), 496-501.

1040 Völker, C., D. W. Wallace, and D. A. Wolf-Gladrow (2002), On the role of heat fluxes in the uptake of  
1041 anthropogenic carbon in the North Atlantic, *Global biogeochemical cycles*, 16(4), 85-81-85-89.

1042 Wassmann, P., C. M. Duarte, S. Agusti, and M. K. Sejr (2011), Footprints of climate change in the Arctic marine  
1043 ecosystem, *Global change biology*, 17(2), 1235-1249.

1044 Webster, N. S., A. P. Negri, E. S. Botté, P. W. Laffy, F. Flores, S. Noonan, C. Schmidt, and S. Uthicke (2016), Host-  
1045 associated coral reef microbes respond to the cumulative pressures of ocean warming and ocean  
1046 acidification, *Scientific Reports*, 6, 19324, doi:10.1038/srep19324  
1047 <https://www.nature.com/articles/srep19324#supplementary-information>.

1048 Zickfeld, K., M. Eby, and A. J. Weaver (2008), Carbon-cycle feedbacks of changes in the Atlantic meridional  
1049 overturning circulation under future atmospheric CO<sub>2</sub>, *Global Biogeochemical Cycles*, 22(3).

1050